J. Plasma Phys. (2026), *vol.* 92, E97 © The Author(s), 2026. Published by Cambridge University Press.
This is an Open Access article, distributed under the terms of the Creative Commons Attribution licence (https://creativecommons.org/licenses/by/4.0/), which permits unrestricted re-use, distribution and reproduction, provided the original article is properly cited. doi:10.1017/S0022377826101986

On the evolution of a large-amplitude, weakly collisional electron plasma wave

Archis Joglekar[1,2,3] and Alec Thomas[3]

[1]Ergodic LLC, Seattle, WA 98103, USA
[2]Pasteur Labs, Brooklyn, NY 11205, USA
[3]Department of Nuclear Engineering and Radiological Sciences, University of Michigan – Ann Arbor, Ann Arbor, MI 48109, USA

Corresponding author: Archis Joglekar, archis@ergodic.io

(Received 4 February 2026 UTC; revision received 25 April 2026 UTC; accepted 1 June 2026 UTC)

Vlasov–Poisson–Fokker–Planck (VPFP) simulations of large-amplitude electron plasma waves, where the bounce frequency is much larger than the collision frequency, $\omega_B \gg \nu_{ee}$, show that the evolution of these waves exhibits three phases: (i) a short-lived trapping phase during which collisional effects are minimal; (ii) a long-lived detrapping phase during which collisional effects are most influential; (iii) a short-lived Landau damping phase where the effect of collisions becomes minimal again. While the dispersion relation during the trapping and Landau damping phase is well known, the wave behaviour during the detrapping phase is not as well understood. The simulations show that during the detrapping phase, the interplay between weak electron–electron collisions and strong wave–electron interactions results in an increasing frequency shift further from the linear root, ω_{EPW}. At the conclusion of the detrapping phase, the distribution function is nearly Maxwellian, the frequency shift rapidly diminishes and the wave damps at a larger rate than the Landau damping rate. Empirical fits to the damping rates, frequency shift enhancement rate and the lifetime of the plasma waves are provided as functions of collision frequency, wavenumber and wave amplitude.

Key words: plasma nonlinear phenomena, plasma waves, plasma simulation

1. Introduction

The dynamics of small-amplitude electron plasma waves (EPWs) is described by the complex root, $\omega_L = \omega_{\mathrm{EPW}} + i\nu_{\mathrm{L}}$, of the linearised dispersion function $\varepsilon(\omega, k_1;\, f(\omega)) = 1 - \omega_p^2 \int f/(\omega - k_1 v)^2 \,\mathrm{d}v$. Assuming a Maxwellian distribution function, EPWs oscillate at a frequency, ω_{EPW}, and damp at the Landau damping rate, ν_{L} (Landau 1946; Canosa 1973). In the case of large-amplitude EPWs, Bernstein, Greene & Kruskal (1957) derived a stationary distribution function where the EPW is sustained due to particle trapping in the potential well of the wave. Such a state, often termed a BGK mode, is described by a nearly Maxwell–Boltzmann distribution function and a nonlinear correction due to quasi-linear diffusion (Davidson 2012) at the phase velocity of the EPW. Manheimer & Flynn (1971), Dewar (1972)

Morales & O'Neil (1972) showed that a BGK mode results in a small negative shift in the wave frequency for a self-consistent solution. In addition to the negative shift in the real part, $\Delta\omega_{NL}$, O'Neil (1965) shows that the imaginary part, i.e. the damping rate, becomes negligible and the dispersion relation is given by $\omega_{NL} = \omega_{\mathrm{EPW}} + \Delta\omega_{\mathrm{NL}} + 0i$. These results rely on constant-amplitude, sudden-turn-on or asymptotic approximations. A more general, non-local, neo-adiabatic framework has since been developed by Bénisti *et al.* (2009), Bénisti (2017*a*,*b*): the damping rate (Bénisti *et al.* 2009), the action distribution function (Bénisti 2017*a*) and the nonlinear frequency shift (Bénisti 2017*b*) of a slowly varying, externally driven EPW are all shown to be history-dependent functionals of the wave amplitude rather than local functions of its instantaneous value. In particular, Bénisti (2017*b*) shows that this non-locality produces a hysteresis in $\delta\omega$ over a grow-then-decay amplitude loop, even in a collisionless plasma. A parallel, collisionless adiabatic framework was developed by Dodin & Fisch (2012*a*,*b*,*c*), Dodin (2014), in which a Whitham-type averaged Lagrangian in oscillation-centre variables yields the nonlinear dispersion relation and frequency shift $\omega_{\mathrm{NL}}(a)$ directly from the trapped-particle distribution. For smooth trapped distributions, this recovers $\omega_{\mathrm{NL}} \propto \sqrt{a}$, but beam-like distributions produce different power laws or a logarithmic nonlinearity and the trapped-particle autoresonance makes ω_{NL} generically non-local. Both the Bénisti and Dodin–Fisch theories are built on the collisionless Vlasov–Poisson system. They describe the Phase I trapping and plateau formation considered later, and, because the slowly-decaying Phase II amplitude keeps the dynamics in their neo-adiabatic regime (the separatrix contraction rate $\dot{v}_{\mathrm{tr}}/v_{\mathrm{tr}} \propto \nu_{\mathrm{eff}}$ is small compared with ω_B), they continue to contribute a collisionless, adiabatic-recession component to the Phase II trapped-particle response. As shown in the remainder of this paper, however, Phase II also requires a Fokker–Planck contribution to the susceptibility: the net nonlinear frequency shift emerges from a self-consistent balance between the collisionless (Vlasov) and collisional (Fokker–Planck) contributions, and cannot be captured by the collisionless frameworks alone.

Previous works assume idealised, collisionless plasmas. Plasmas accessible in the laboratory, e.g. those in fusion and gas discharge experiments, and in Nature, e.g. in the ionosphere and the interstellar medium, are often weakly collisional such that the ratio of $\nu_{ee}/\omega_p \sim 10^{-4}{-}10^{-10}$, where ν_{ee} is the electron–electron (e–e) collision frequency (Thorne & Blandford 2017). While it is implicitly known that in collisional systems, BGK modes cannot persist forever and that over time, the wave must exhibit some damping as the particles thermalise, the dynamics of this transition from nonlinear to the linear state is not well understood.

Using asymptotic analysis, Zakharov & Karpman (1963) (ZK) determined that during the detrapping phase, the effective damping rate in weakly collisional, nonlinear EPW can be given by $\nu_{\mathrm{ZK}} \propto (\nu_{ee}\omega_{\mathrm{EPW}}^2/\omega_B^3)\nu_{\mathrm{L}}$, where ν_{ee} is the e–e collision frequency, ω_{EPW} is the linear resonance, ω_B is the bounce frequency of the trapped particles, ν_L is the linear Landau damping rate. While the calculation of this relation contains approximations e.g. fluid Landau damping rate, it correctly suggests that waves can have effective damping rates larger than the base e–e collision rate because the rate is inversely proportional to ω_B/ω_p. Numerical verification of this has been limited to a few simulations using a Particle-In-Cell code where the simulations found qualitative agreement (Valentini 2008).

This paper provides an end-to-end description of the wave dynamics in weakly collisional, large-amplitude EPWs which exhibits three distinct phases. Phase I comprises well-understood collisionless mechanisms of wave excitation, particle trapping

https://doi.org/10.1017/S0022377826101986 Published online by Cambridge University Press

Phase	m in $\mathcal{O}(E^m)$	n in $\mathcal{O}(\nu_{ee}^n)$	Re(ω)	Im(ω)
I	2	0	$\omega_{\mathrm{EPW}} + \Delta\omega_{\mathrm{NL}}$	0
II	2	1	$\omega_{\mathrm{EPW}} + \Delta\omega_{\mathrm{NL}} \exp(\gamma_{\Delta\omega} t)$	$f_{\mathrm{NL}}\, \nu_{\mathrm{L}}$
III	1	0	ω_{EPW}	$f_{\mathrm{L}}\, \nu_L$

TABLE 1. Three distinct phases of nonlinear electron plasma wave evolution are framed in terms of perturbative expansions necessary to describe each phase as well as the resulting dispersion relation of each phase. The second and third columns give respectively the lowest order m in wave amplitude E and order n in collision frequency ν_{ee} at which the dispersion-relation contributions in that phase appear.

and the establishment of a quasi-linear plateau. The physics in this phase can be described by a second-order perturbative expansion of the Vlasov–Poisson system with the electric field, E, as the small parameter. Phase II is the longest-lived phase during which a quasi-steady state is reached between weak electron–electron collisions and strong wave–electron interactions. Describing Phase II requires a first-order expansion in ν_{ee} as another small parameter in addition to the second-order expansion in E. The wave evolution concludes with Phase III when the distribution function has returned to a near-Maxwellian and the wave energy is rapidly damped via Landau damping. Only the first-order expansion in E is required to describe this phase accurately. While the behaviour in Phases I and III has previously been elucidated, this work describes collisional effects on the wave dispersion relation during Phase II and characterises the lifetime of Phase II. With these quantities, weakly collisional, large-amplitude EPW can be modelled as a piecewise ordinary differential equation.

The remainder of this paper is organised as follows. Section 2 describes the simulation configuration. Section 3 provides an overview of the overall wave dynamics, and introduces the three distinct phases of evolution and highlights the enhancement of the nonlinear frequency shift during the detrapping phase. Section 4 describes the physical mechanism for this enhancement of the nonlinear frequency shift. Sections 5, 6 and 7 describe each phase in detail along with empirical fits for the quantities described in table 1. Finally, § 8 summarises the findings and discusses future work.

2. Simulation configuration

Weakly collisional, large amplitude electron plasma waves are studied using a 1-D1V Eulerian Vlasov–Poisson–Fokker–Planck solver (Joglekar & Levy 2020) with periodic boundary conditions. The equations that are solved are given by

$$\frac{\partial f}{\partial t} + v\frac{\partial f}{\partial x} - \frac{q}{m}E\frac{\partial f}{\partial v} = \nu_{ee}\,\mathcal{C}(f), \tag{2.1}$$

$$\frac{\partial E}{\partial x} = \frac{q}{\varepsilon_0}\left(\int_{-\infty}^{\infty} f\,\mathrm{d}v - n_0\right). \tag{2.2}$$

While Particle-In-Cell methods are a common tool for studying plasma kinetic behaviour, the slow convergence with particle number is a problem for resolving subtle, kinetic phenomena. In these simulations, $N_x = 256$, $N_v = 2048$,

https://doi.org/10.1017/S0022377826101986 Published online by Cambridge University Press

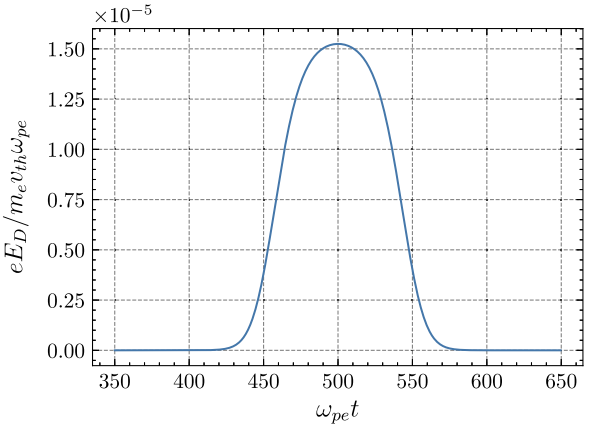


FIGURE 1. Envelope amplitude of the external forcing term over time. This value is then multiplied by $\sin(kx - \omega_{\mathrm{EPW}}t)$ to give the external forcing term on the space–time grid.

$L_x = 2\pi/k\lambda_D$, $\Delta t = 0.5$, $\omega_{pe}t_{\max} = 4000$. Exponential integrators with spectral derivatives in position and velocity space for the different components of the Vlasov equation are used (Thomas 2016). The simulations step through the phase-space integrators with a 6th-order integrator in time. Poisson's equation is solved using a spectral solver. The advection–diffusion Fokker–Planck equation (Dougherty 1964), $\mathcal{C}(f) = (\partial/\partial v)(\bar{v}f + \langle v - \bar{v}\rangle^2(\partial f/\partial v))$, is solved using a first-order Euler implicit solver with centre differencing of the velocity derivatives. The distribution function is initialised uniformly in space, that is, the density and temperature profiles are uniform. The distribution function is initially Maxwellian.

EPWs are driven using a ponderomotive driver as shown by Joglekar & Thomas (2023). Because a Hilbert transform of the electric field is necessary for determining the time-dependent oscillation frequency, the driver is started $450\omega_p^{-1}$ into the simulation. This prevents the noise that the Hilbert transform introduces into the beginning and end of the transformed signal from obfuscating the changing frequency during the drive phase and Phase I. The parameters for the time envelope are $t_c = 500\omega_p^{-1}$, $t_w = 100\omega_p^{-1}$, $t_R = 25\omega_p^{-1}$, $\omega = \omega_{\mathrm{EPW}}(k\lambda_D)$. This results in a driver profile given in figure 1. The amplitude of this driver profile is multiplied by $\sin(kx - \omega_{\mathrm{EPW}}t)$, where ω_{EPW} is given by the solution to the linearised dispersion relation for small amplitude EPWs.

Here, 1600 simulations are performed by scanning over

$$0.3 \leqslant k\lambda_D \leqslant 0.35, \tag{2.3}$$

$$0.005 \leqslant a_0 \leqslant 0.02, \tag{2.4}$$

$$10^{-5} \leqslant \nu_{ee} \leqslant 10^{-3.5}, \tag{2.5}$$

in 10, 10 and 16 steps, respectively. The parameter ranges were chosen to ensure all three phases are observable within computationally tractable simulation times. For $k\lambda_D < 0.3$, weak Landau damping requires either very long simulations or smaller amplitudes to observe Phase III. For $k\lambda_D > 0.35$, strong damping necessitates larger amplitudes, which would push portions of the parameter space into either purely linear or purely nonlinear regimes.

https://doi.org/10.1017/S0022377826101986 Published online by Cambridge University Press

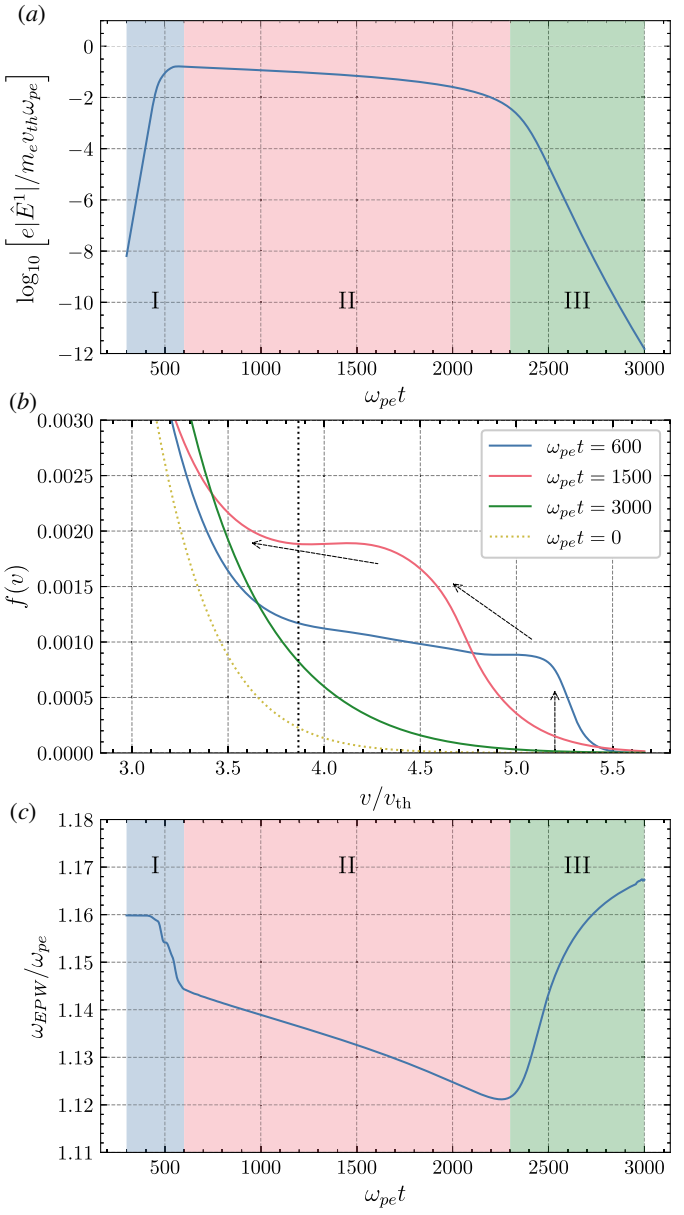


FIGURE 2. (*a*) Wave amplitude, (*b*) spatially averaged distribution function and (*c*) wave oscillation frequency are plotted during three distinct phases of wave evolution. The vertical dotted line in panel (*b*) indicates the EPW phase velocity $v_{\rm ph}$.

The following section discusses power-law fits to data collected from the 1600 simulations and attempts to explain the dynamics that surface in those data.

3. Overall wave dynamics

Figure 2 shows the three distinct phases of weakly collisional, large-amplitude EPW evolution. Figure 2(*a*) shows the evolution of the wave amplitude. Phase I is

https://doi.org/10.1017/S0022377826101986 Published online by Cambridge University Press

very short-lived, as it encompasses the relatively fast dynamics of wave excitation and particle trapping. The dynamics is primarily collisionless, where wave damping is diminished due to quasi-linear diffusion (Bernstein *et al.* 1957; O'Neil 1965; Davidson 2012) and there is a corresponding shift in the frequency of oscillation of the wave (Manheimer & Flynn 1971; Dewar 1972; Morales & O'Neil 1972; Berger *et al.* 2013). Figure 2(*b*) shows the spatially averaged distribution function $|\hat{f}^0|(v)$ in the trapping region. During Phase I, it exhibits flattening at the phase velocity of the wave, as expected via quasi-linear diffusion. It also exhibits heating of the particles in a region $\approx \pm 1.5 v_{\mathrm{tr}}$ from the phase velocity, where the trapping velocity $v_{\mathrm{tr}} = \sqrt{2E/k}$ and particularly where $v > v_{\mathrm{ph}} + v_{\mathrm{tr}}$. The two velocity scales play distinct roles: $v_{\mathrm{ph}} = \omega/k$ is the wave-frame location of the resonant region and is amplitude-independent, while v_{tr} is the amplitude-dependent half-width of the separatrix about v_{ph}. This modification of the distribution function in the trapping region results in the well-established nonlinear frequency shift where the EPW frequency downshifts by a few percent as shown in figure 2(*c*).

During Phase II, figure 2(*a*) shows that the wave amplitude is weakly damped. Data from simulations indicate that the rate is lower than the Landau damping rate, but higher than the collision frequency. In figure 2(*b*), it is seen that the distribution function has developed a plateau at the phase velocity. The plateau spans the trapping region, with width $\approx 2v_{\mathrm{tr}}$, which slowly shrinks during Phase II as the wave damps and $v_{\mathrm{tr}} = \sqrt{2E/k}$ decreases. The slope $\partial f/\partial v$ at v_{ph} remains small relative to the Maxwellian value but is finite, consistent with the weak, nearly constant damping rate observed in figure 2(*a*). Compared with the distribution function in Phase I, there are more particles in the trapping region and fewer particles in $v > v_{\mathrm{ph}} + v_{\mathrm{tr}}$. During this time, the wave frequency clearly decreases, exhibiting a further shift away from the value dictated by linear behaviour, $\omega_{\mathrm{EPW}} = 1.16$.

After $> \mathcal{O}(100)$ bounce periods, figure 2(*a*), the damping rate increases rapidly to the order of the Landau damping rate. This indicates the beginning of Phase III. Figure 2(*b*) shows that the trapped particles have thermalised and the distribution function has become nearly Maxwellian. Consequently, figure 2(*c*) shows that the EPW frequency reverts to that of a small-amplitude, slightly warmer and strongly damped EPW.

The effects on the dispersion relation during the three phases are summarised in table 1, where ω_{EPW} and ν_L are the real and imaginary part of the solution to the linearised dispersion relation, respectively. It is found that for $0.3 \leqslant k\lambda_D \leqslant 0.35$, $0.1 < \omega_B < 0.25$ and $10^{-5} < \nu_{ee} < 3 \times 10^{-4}$, the dynamics can be described by using the set of quantities described in the equations in the table.

Table 2 provides empirical fits for the quantities described in table 1 as power-laws of the form $Q = C(k\lambda_D)^{\alpha}(\omega_B)^{\beta}(\nu_{ee})^{\gamma}$, where C, α, β, γ are fit parameters. Each of the fits has an $R^2 > 0.95$ in real and log space indicating that the empirical power laws work well for the parameter space studied here.

The next section focuses on the novel physics in these simulations, the increase in the nonlinear frequency shift due to collisions during Phase II. The subsequent sections describe the dynamics in each phase in detail and provide empirical fits for the quantities described in table 1.

4. Physical mechanism for frequency shift enhancement

To determine the reason for the counter-intuitive increase in the frequency shift, the contribution to the dielectric function from the evolution operators in the Vlasov–Poisson–Fokker–Planck (VPFP) system of equations can be calculated.

https://doi.org/10.1017/S0022377826101986 Published online by Cambridge University Press

Quantity	Coefficient	$\alpha(k\lambda_D)$	$\beta(\omega_B)$	$\gamma(\nu_{ee})$	R^2
$\Delta\omega_{NL}$	93.00 ± 1.75	5.92 ± 0.01	0.81 ± 0.00	0.06 ± 0.00	0.99
$\gamma_{\Delta\omega}$	0.03 ± 0.00	-0.93 ± 0.06	-0.88 ± 0.01	0.80 ± 0.00	0.97
f_{NL}	9.51 ± 0.87	-1.43 ± 0.07	-1.48 ± 0.02	1.07 ± 0.00	0.99
τ_{II}	0.13 ± 0.01	-3.82 ± 0.03	1.23 ± 0.01	-0.86 ± 0.00	0.99
f_L	1.73 ± 0.18	-2.25 ± 0.06	0.78 ± 0.01	0.15 ± 0.01	0.92

TABLE 2. Best fits for the quantities described in table 1 as power-laws of the form $Q = C(k\lambda_D)^{\alpha}(\omega_B)^{\beta}(\nu_{ee})^{\gamma}$, where C, α, β, γ are fit parameters. Uncertainties <0.005 are reported as 0.00.

The evolution equation of quasi-linear theory (Davidson 2012) for the spatially averaged distribution for a one-component collisional, unmagnetised plasma can be written as

$$\frac{\partial \hat{f}^0}{\partial t} + \frac{q}{m}\left(\hat{E}^{1\star}\frac{\partial \hat{f}^1}{\partial v} + \hat{E}^1\frac{\partial \hat{f}^{1*}}{\partial v}\right) = \nu_{ee}\,\mathcal{C}(\hat{f}^0). \tag{4.1}$$

Performing a perturbative expansion assuming $\nu_{ee} \ll \omega_B$, that is, the collision frequency is much smaller than the bounce frequency, and using $\hat{f}^0 = \hat{f}^0_0 + \nu_{ee}\hat{f}^0_1$ where the subscript indicates the order in ν_{ee}, (4.1) becomes

$$\frac{\partial \hat{f}^0_0}{\partial t} + \frac{q}{m}\left(\hat{E}^{1\star}_0\frac{\partial \hat{f}^1_0}{\partial v} + \hat{E}^1_0\frac{\partial \hat{f}^{1\star}_0}{\partial v}\right) = 0, \tag{4.2}$$

$$\frac{\partial \hat{f}^0_1}{\partial t} + \frac{q}{m}\left(\hat{E}^{1\star}_0\frac{\partial \hat{f}^1_1}{\partial v} + \hat{E}^1_1\frac{\partial \hat{f}^{1\star}_0}{\partial v}\right) = \hat{C}(\hat{f}^0_0). \tag{4.3}$$

Equation (4.2) can be written as the quasilinear diffusion equation that leads to the well-understood collisionless dynamics of the flattening of the distribution function and the nonlinear frequency shift of Phase I. Equation (4.3) is the weakly collisional perturbative correction to the collisionless spatially averaged distribution function $\hat{f}^0_0$. It is $\hat{f}^0_1$ that is responsible for the increase in the frequency shift. That is, the collisional perturbation to the distribution function leads to an enhancement of the nonlinear frequency shift.

This can be formalised by using the dielectric function given by $\varepsilon(\omega; k_1) = 1 - \omega_p^2 \int_{-\infty}^{\infty} \hat{\tilde{f}}^0/(\omega - k_1 v)^2\,\mathrm{d}v$, where $\hat{\tilde{f}}^0 = \hat{f}^0/n_0$ and n_0 is the plasma density, with $\omega_p^2 = q^2 n_0/m\varepsilon_0$. If $\hat{\tilde{f}}^0 = \tilde{f}_M$, a Maxwellian distribution, the linear wave dispersion relation has the real frequency ω_1, which is the solution to $\varepsilon(\omega_1; k_1) = 0$. If the dispersion function is expanded about the linear frequency for $\omega = \omega_1 + \delta\omega$, to lowest order, $\delta\omega = \omega_p^2[(\partial\varepsilon/\partial\omega)|_{\omega=\omega_1}]^{-1}\int_{-\infty}^{\infty}(\delta\hat{f}^0)/(\omega_1 - k_1 v)^2\,\mathrm{d}v$, i.e. the nonlinear change in $\hat{f}^0$ from the coupling of $\hat{f}_1$ to the field leads to a well-known frequency shift (Manheimer & Flynn 1971; Dewar 1972; Morales & O'Neil 1972).

The time derivative of the frequency shift is

$$\frac{\partial}{\partial t}\delta\omega = \omega_p^2\left[\left.\frac{\partial\varepsilon}{\partial\omega}\right|_{\omega=\omega_1}\right]^{-1}\int_{-\infty}^{\infty}\frac{1}{(\omega_1 - k_1 v)^2}\frac{\partial\hat{\tilde{f}}_0}{\partial t}\,\mathrm{d}v, \tag{4.4}$$

https://doi.org/10.1017/S0022377826101986 Published online by Cambridge University Press

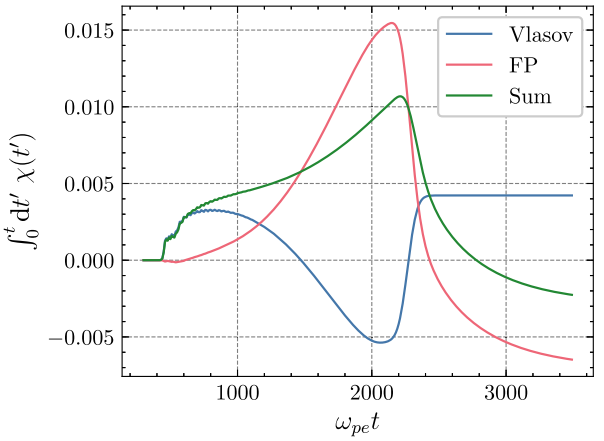


FIGURE 3. Evolution of the contributions to the susceptibility function.

with $\partial \hat{\tilde{f}}_0/\partial t$ given by (4.1) which includes the fast time scale rate of evolution from the normal quasilinear theory (Davidson 2012) and the slow collisional relaxation of the distribution function. Expanding (4.4) in ν_{ee} gives

$$\frac{\partial(\delta\omega_0 + \nu\delta\omega_1)}{\partial t} = \left[\left.\frac{\partial\varepsilon}{\partial\omega}\right|_{\omega=\omega_1}\right]^{-1}\left[\chi\left(\partial_t \hat{f}_0^0\right) + \nu\chi\left(\partial_t \hat{f}_1^0\right)\right], \tag{4.5}$$

where $\chi(f) = \omega_p^2 \int f/(\omega_1 - k_1 v)^2\,\mathrm{d}v$ is the susceptibility function.

The first term on each side represents the frequency shift described by Manheimer & Flynn (1971), Dewar (1972), Morales & O'Neil (1972). The second term is the collisional contribution and is given by substituting (4.3) for $\partial_t \hat{f}_1^0$, which gives

$$\frac{\partial\delta\omega_1}{\partial t} = \left[\left.\frac{\partial\varepsilon}{\partial\omega}\right|_{\omega_1}\right]^{-1}\chi\left(\mathcal{V}\left(\hat{f}_0^1, \hat{f}_1^1\right)\right) - \chi\left(\mathcal{C}\left(\hat{f}^0\right)\right), \tag{4.6}$$

where $\mathcal{V}(f_0^1, f_1^1) = E_0^{1*}(\partial f_1^1/\partial v) + E_1^{1*}(\partial f_1^1/\partial v) + \text{c.c.}$ is the linearised contribution from the Vlasov terms in (4.1) and $E^1 = E_0^1 + \nu E_1^1$. By using this relation, the effect on the dielectric function of the Vlasov terms and the Fokker–Planck terms can be isolated and compared. This comparison is performed numerically in fully nonlinear VPFP simulations with a Dougherty collision operator (Dougherty 1964), given by $\mathcal{C}(f) = \partial_v(\bar{v}f + \bar{v}_{\text{th}}^2\partial_v f)$, where $\bar{v} = \int \mathrm{d}v\ v\ f$ and $\bar{v}_{th}^2 = \int \mathrm{d}v\ (v - \bar{v})^2\ f$. This collision operator conserves density, momentum and energy, and performs a linearised approximation of the phase-space drag and diffusion from small-angle collisions.

Figure 3 compares the change in the dielectric function, $\Delta\epsilon$, from the Vlasov terms to $\Delta\epsilon$ from the collision operator. It shows that during Phase I, the Vlasov contribution dominates as expected from the theory from Manheimer & Flynn (1971), Dewar (1972), Morales & O'Neil (1972). However, during Phase II, the quasi-steady equilibrium between the Vlasov and Fokker–Planck term is responsible for a net increase in the frequency shift. The Fokker–Planck term always has a positive contribution while the Vlasov contribution counteracts this behaviour, but only partially, resulting in a net increase in the frequency shift of the EPW. The subsequent increase can be roughly equal in magnitude to the initial collisionless nonlinear frequency shift from Phase I. This behaviour is persistent over all simulations.

https://doi.org/10.1017/S0022377826101986 Published online by Cambridge University Press

Simulation	ν_{ee}/ω_{pe}
A	10^{-5}
B	10^{-4}
C	1.2×10^{-4}
D	3.6×10^{-4}

TABLE 3. Simulations used in the remainder of the manuscript have the same $k\lambda_D = 0.3$ and drive strength a_0, and varying collision frequencies ν_{ee}.

Physically, the collision operator continuously scatters particles at the edges of the trapping region. If the particle trapping is not saturated, there will remain a negative slope at the phase velocity of the wave and wave–particle interactions continue to occur. This quasi-steady competition results in a net redistribution of phase space density that contributes positively to the susceptibility function. The precise mechanism by which this balance produces an enhanced frequency shift, rather than simply restoring linear behaviour, remains an open question for future theoretical work.

In the sections that follow, each phase is described in detail along with empirical fits for the quantities described in table 1.

5. Phase I: trapping and plateau formation

Phase I is a short-lived phase that encompasses wave excitation and particle trapping. The modifications to the dispersion relation include the loss of wave damping and a nonlinear frequency shift. In the following sections that describe each phase in detail, four simulations, each with $k\lambda_D = 0.3$, $a_0 = 0.1$ and varying collision frequencies are used as examples. These are given in table 3.

5.1. *Phase space evolution*

During Phase I, particles near the phase velocity of the wave are trapped in the potential well. This creates a phase space vortex near the phase velocity of the wave.

Phase space snapshots at $\omega_{pe}t = 650$ are shown in figure 4(*a*) for Simulations A and B. Both snapshots show a similarly sized vortex. This is because the effect of weak collisions and Landau damping has not yet surfaced and the wave amplitudes are nearly the same. However, the snapshot from Simulation B exhibits more smoothing throughout and the features are not as sharp, especially near the edges of the trapping region.

Figure 4 also shows that both waves are roughly in phase with one another, as indicated by the fact that the vortex is centred around $10\lambda_D$ in both cases.

5.2. *Wave evolution and nonlinear frequency shift*

The wave evolution early in time in Simulations A and B is plotted in figure 5(*a*). It shows that the magnitudes of the driven waves in both simulations are within a few percent of one another and only weakly affected by collisions. However, there are two differences that should be highlighted.

The first is that the effect of the weak damping is already evident in the first $200\omega_{pe}t$ of the simulation after the drive is turned off around $600\omega_{pe}t$. The difference in the damping rates is clear in figure 5(*a*), where the wave amplitude in Simulation

https://doi.org/10.1017/S0022377826101986 Published online by Cambridge University Press

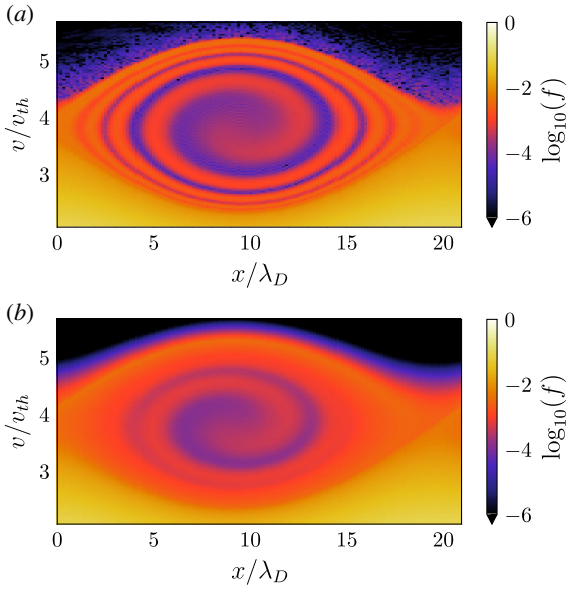


FIGURE 4. Phase space portrait at $t = 650\omega_{pe}^{-1}$, shortly after the drive is turned off, for Simulations A and B.

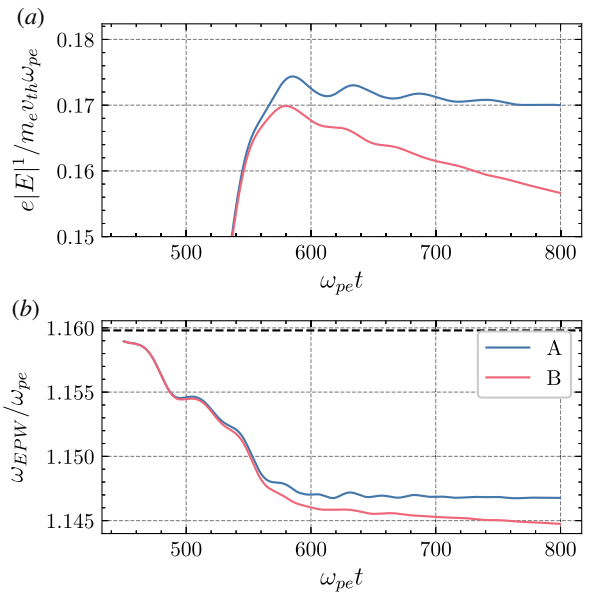
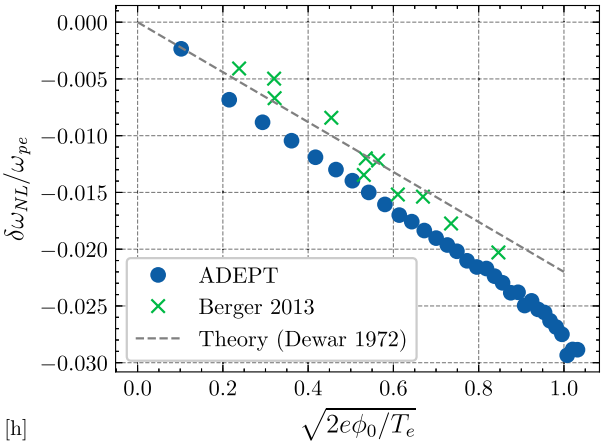


FIGURE 5. Evolution of the (*a*) wave amplitude (*b*) and instantaneous frequency during Phase I for Simulations A and B. The dashed line in panel (*b*) indicates the linear frequency.

B decays faster than that in Simulation A. The instantaneous frequency of the wave is plotted in figure 5(*b*) and shows similar behaviour in that the initial frequency shifts are within a few percent of each other, but the decrease in the frequency as the wave amplitude is damped in Simulation B is evident.

https://doi.org/10.1017/S0022377826101986 Published online by Cambridge University Press



[h]

FIGURE 6. Nonlinear frequency shift versus normaliesd wave amplitude. Data from ADEPT and Berger *et al.* (2013) along with the theoretical curve (line) from Dewar (1972) are compared.

Second, the oscillations in the wave amplitude corresponding to particle trapping are suppressed faster in Simulation B. This is likely due to the additional smoothing of the vortex that is evident in figure 4. Similar to the wave amplitude behaviour, the bounce oscillations in the wave frequency are suppressed more quickly in Simulation B.

The nonlinear frequency shift during Phase I is measured by performing a Hilbert transform of the electric field to extract the instantaneous frequency of oscillation. The frequency shift, $\Delta\omega = \omega - \omega_{\mathrm{EPW}}$, is measured at the end of Phase I, which is defined as the time when the wave amplitude reaches its first maximum after the drive has been turned off. Fitting the data from all 1600 simulations results in the empirical relation given by

$$\Delta\omega = 93.00 \pm 1.75\,(k\lambda_D)^{5.92\pm0.01}\,\omega_B^{0.81\pm0.00}\,\nu_{ee}^{0.06\pm0.00}, \tag{5.1}$$

where $\omega_B = \sqrt{kE}$ is the bounce frequency of the trapped particles. This fit has an R^2 value of 0.996 indicating excellent agreement with the data.

The nonlinear frequency shift given by (5.1) has a strong dependence on $k\lambda_D$ because the frequency shift is a direct result of the rearrangement of the phase space density. The phase space density is a strong function of the phase velocity of the wave which is a strong function of $k\lambda_D$.

The fact that Phase I comprises collisionless dynamics is also reflected in the effectively negligible dependence on the collision rate in (5.1).

Finally, (5.1) has a weaker dependence on the wave amplitude than that reported by Manheimer & Flynn (1971), Dewar (1972), Morales & O'Neil (1972), Berger *et al.* (2013), where $\Delta\omega \propto \omega_B$. While an analytical derivation of this scaling is outside the scope of this work, comparisons to prior simulations and theory are performed. Figure 6 shows a direct comparison to the plot of Berger *et al.* (2013). The data from ADEPT agree well with the data from Berger *et al.* (2013) and both datasets are within a few percent of the theoretical curve of Dewar (1972). This figure suggests that ADEPT is performing similarly to the Vlasov code used by Berger *et al.* (2013) and that the discrepancy between the measured scaling and the theoretical scaling is not due to numerical artefacts, but rather due to the approximations used in

https://doi.org/10.1017/S0022377826101986 Published online by Cambridge University Press

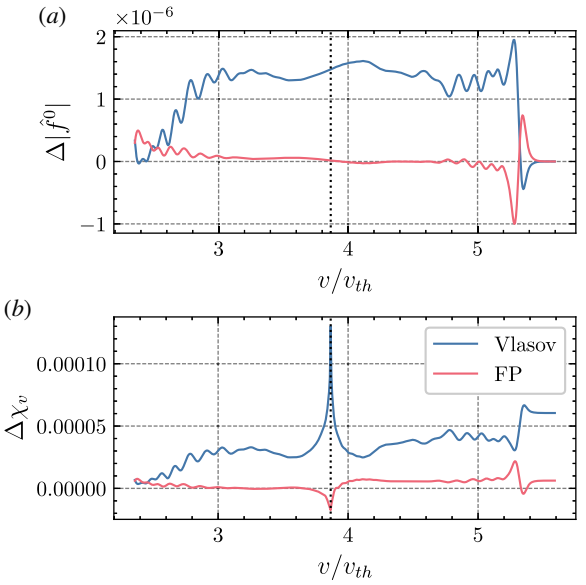


FIGURE 7. (*a*) Contribution to $\Delta|\hat{f}^0(v)|$ integrated over the first $\omega_{pe}t = 600$. (*b*) Corresponding contribution to $\Delta\chi(v)$, which is directly proportional to $\Delta|\hat{f}^0|$.

the derivation of the theory. Further, Berger *et al.* (2013) noted that the measured nonlinear frequency shift is sensitive to the specifics of the drive duration.

It is also important to consider that the linear scaling was derived using asymptotic approximations by Manheimer & Flynn (1971), Dewar (1972), Morales & O'Neil (1972). Specifically, Morales & O'Neil (1972) stipulate that $v_{tr}v_{ph} \ll v_{th}^2$. In these simulations, $v_{ph} \approx 3.3v_{th}$ and $v_t r \gtrapprox 0.5$. They also stipulate that their theory requires $v_p h \geqslant 4v_{th}$, which leads to $k\lambda_D < 0.3$. In these simulations, $0.3 \leqslant k\lambda_D \leqslant 0.35$. These violations of the assumptions used in the derivation of the theory could explain the discrepancy in the scaling with wave amplitude, while the close agreement with previous simulations as well as the theoretical curve in figure 6 suggest that the simulations are reasonably accurately capturing the nonlinear frequency shift physics.

5.3. *Physical mechanism for the nonlinear frequency shift*

Figure 7(*a*) distinguishes the change in the spatially averaged distribution function over the first 600 $\omega_{pe}t$ from the Vlasov terms and the Fokker–Planck terms. It shows that the Vlasov terms cause a substantial increase in density in the trapping region, while the contribution from the Fokker–Planck terms is negligible.

Figure 7(*b*) shows the corresponding contribution to the susceptibility function, $\Delta\chi(v) = \omega_{pe}^2 \int_0^v \partial_v' \Delta|\hat{f}^0(v')|/(\omega - kv')\,\mathrm{d}v'$, which is directly proportional to the frequency shift. The different contributions are calculated by summing the change in the distribution function from each of the terms in the simulations. It shows that the Vlasov terms are responsible for the nonlinear frequency shift, while the Fokker–Planck terms have a negligible effect. This confirms that the nonlinear frequency shift during Phase I is a collisionless effect arising from wave–particle interactions, as expected from Manheimer & Flynn (1971), Dewar (1972), Morales & O'Neil (1972), Berger *et al.* (2013).

https://doi.org/10.1017/S0022377826101986 Published online by Cambridge University Press

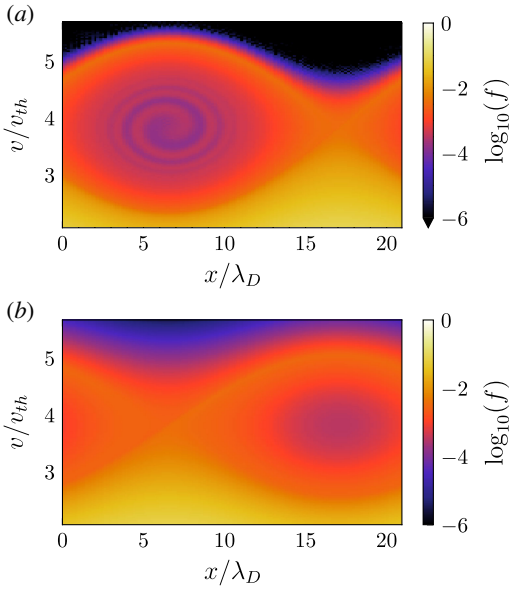


FIGURE 8. Phase space portrait at $t = 1400\omega_{pe}^{-1}$, long after the drive is turned off, for two different collision frequencies.

6. Phase II: quasi-steady collisional phase

Phase II is the longest-lived phase during which a quasi-steady state between weak electron–electron collisions and strong wave–electron interactions governs the dynamics. Figures 2(*a*) and 2(*c*) suggest that the wave evolution during this phase is characterised by three quantities; the effective damping rate of the wave, the growth rate of the nonlinear frequency shift and the lifetime of Phase II. Each of these quantities is discussed in the following subsections. First, the phase space evolution during this phase is described.

6.1. *Phase space evolution*

Figures 8(*a*) and 8(*b*) show phase space snapshots during Phase II for Simulations A and Simulation B, respectively, at $\omega_{pe}t = 1400$.

The snapshots show that similarly sized vortices persist in both simulations despite the wave amplitude in Simulation B being roughly half that of Simulation A.

Simulation B exhibits substantial phase space diffusion to the extent that the trapped particle orbits are not discernible as they are in Simulation A. This is because the higher collision frequency in Simulation B leads to more rapid phase space diffusion in the deeply trapped region where the gradients in velocity space are large.

It is also evident from figure 8 that there is a phase shift between the two simulations. This is because the wave frequency has experienced a greater downshift in Simulation B due to the effect highlighted in the previous section.

6.2. *Wave amplitude and frequency evolution*

Figure 9(*a*) shows the evolution of the electric field amplitude over a longer time scale for all four simulations. The monotonic increase of the effective damping rate

https://doi.org/10.1017/S0022377826101986 Published online by Cambridge University Press

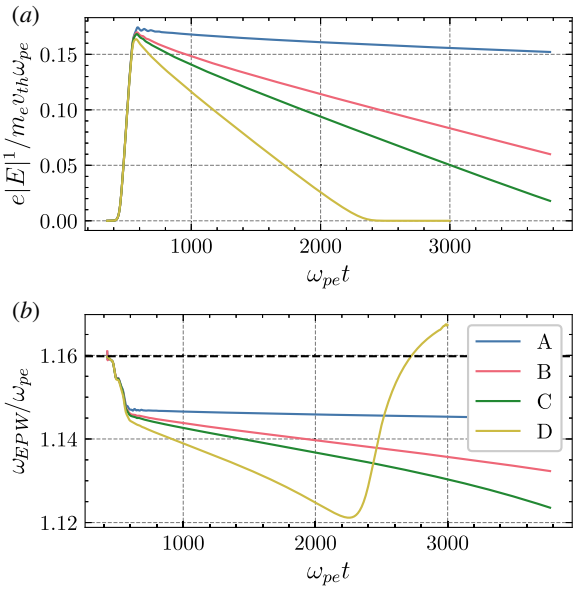


FIGURE 9. Evolution of the (*a*) wave amplitude and (*b*) wave frequency for four different collision frequencies. Simulation D, which has the largest ν_{ee} and therefore the shortest Phase II lifetime (6.3), enters Phase III near $\omega_{pe}t \approx 2300$ within the displayed window, visible as the rapid drop in amplitude in panel (*a*) and the rapid rise in frequency back toward ω_{EPW} in panel (*b*); see § 7.

with ν_{ee} has two complementary physical origins. At the linear level, the Lenard–Bernstein treatment of the Vlasov–Fokker–Planck dispersion relation (Lenard & Bernstein 1958) predicts that the bare collision frequency simply augments the Landau rate, $\nu_{\mathrm{eff}} \approx \nu_L + \mathcal{O}(\nu_{ee})$, so more collisions mean more damping. In the large-amplitude regime considered here, however, trapping would otherwise largely suppress the Landau contribution (O'Neil 1965); the Phase II damping rate instead reflects the efficiency with which collisions scatter particles across the separatrix and reinstate a Landau-like kinetic response. The near-linear-in-ν_{ee} scaling of the effective damping rate in the trapped regime was first derived by Zakharov & Karpman (1963) via an asymptotic boundary-layer analysis of the separatrix (introduced in § 1; the quantitative comparison with our fits is given later in this section). More recently, Berger *et al.* (2023) have recast the same trapping–detrapping competition as a binary amplitude-threshold criterion, $\omega_B \tau_c \sim 2\pi$: above threshold, bounce motion wins and $\nu_{\mathrm{eff}} \ll \nu_L$, while increasing ν_{ee} at fixed ω_B drives the wave towards the threshold and ν_{eff} accordingly grows towards ν_L. The Phase II rates in figure 9(*a*) sit between ν_{ee} and ν_L for all four simulations, consistent with this picture – neither the bare collision rate nor the linear Landau rate describes the dynamics in isolation. Bounce oscillations have been suppressed over this time scale. Of the four simulations, only Simulation D reaches Phase III within the displayed window: its amplitude in figure 9(*a*) begins to decrease rapidly after $\omega_{pe}t \approx 2300$, marking the onset of the collisional return to Landau damping analysed in § 7. This is consistent with (6.3): Simulation D has the largest ν_{ee} in the scan and therefore the shortest Phase II lifetime, so it is the first to exit Phase II.

https://doi.org/10.1017/S0022377826101986 Published online by Cambridge University Press

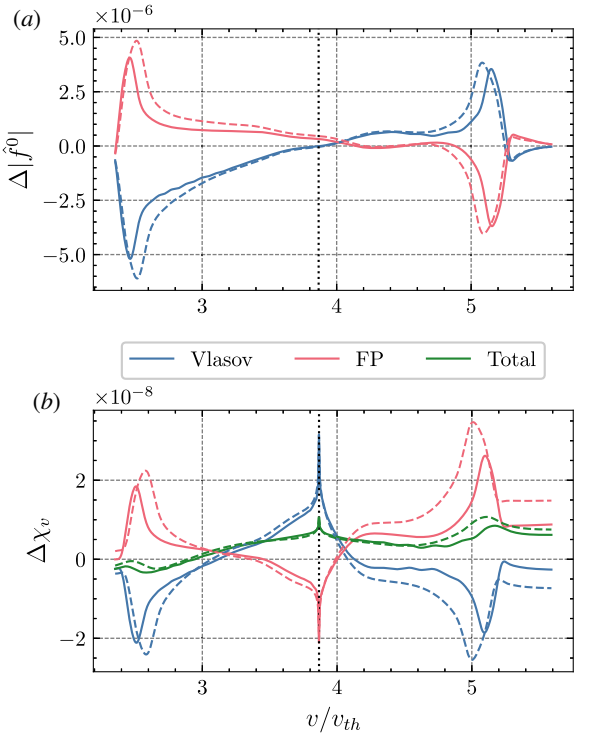


FIGURE 10. (*a*) Change in phase space density $\Delta|\hat{f}^0(v)|$ over Phase II from the different terms. (*b*) Corresponding contributions to the susceptibility function $\Delta\chi(v)$ and the sum. Solid, Sim A; dashed, Sim B.

Figure 9(*b*) shows the corresponding evolution of the instantaneous frequency of the wave. It shows that the frequency can downshift substantially during Phase II and that the rate of downshift increases with increasing collision frequency. Mirroring the amplitude behaviour in panel (*a*), the frequency in Simulation D begins to rapidly increase after $\omega_{pe}t \approx 2300$ and returns towards the linear value ω_{EPW}; this is the Phase III signature of the re-Maxwellianisation of the distribution function, and is analysed in detail in § 7. This is the same Simulation D used throughout the manuscript as the reference three-phase evolution shown in figure 2.

6.3. *Physical mechanism for frequency shift enhancement*

Figure 10(*a*) distinguishes the change in the spatially averaged distribution function over the first 600 $\omega_{pe}t$ from the Vlasov terms and the Fokker–Planck terms. It shows that the Vlasov terms redistribute the phase space density from slower velocities to faster velocities while the Fokker–Planck terms do the opposite. The net result, not shown here due to space constraints, is a slight increase in phase space density in the trapping region above the phase velocity.

Figure 10(*b*) shows the corresponding contribution to the susceptibility function. It shows that the Vlasov terms, in blue, are responsible for a net decrease in the frequency shift, while the Fokker–Planck terms, in red, are responsible for a net increase in the frequency shift. The net result, in green, is an increase in the frequency shift during Phase II.

https://doi.org/10.1017/S0022377826101986 Published online by Cambridge University Press

The dashed lines in figure 10 are the results from Simulation B. It shows similar behaviour to Simulation A, but the magnitudes of the contributions are larger due to the higher collision frequency. A larger increase in phase space density in the trapping region results in a larger increase in the frequency shift.

6.4. *Summary of Phase II dynamics*

In Phase II, the growth rate of the nonlinear frequency shift, the effective damping rate of the wave and the lifetime of Phase II are given by

$$\gamma_{\Delta\omega} = 0.03 \pm 0.00 \, \frac{\nu_{ee}^{0.80\pm0.00}}{(k\lambda_D)^{0.93\pm0.06}\, \omega_B^{0.88\pm0.01}}, \tag{6.1}$$

$$f_{\mathrm{NL}} = 9.51 \pm 0.87 \, \frac{\nu_{ee}^{1.07\pm0.00}}{(k\lambda_D)^{1.43\pm0.07}\, \omega_B^{1.48\pm0.02}}, \tag{6.2}$$

$$\tau_{\mathrm{II}} = 0.13 \pm 0.01 \, \frac{\omega_B^{1.23\pm0.01}}{(k\lambda_D)^{3.82\pm0.03} \nu_{ee}^{0.86\pm0.00}}, \tag{6.3}$$

respectively. Equations (6.1) and (6.2) vanish as $\nu_{ee} \to 0$ and the collisionless dynamics of Phase I are recovered. Collisionless behaviour prescribes a persistent wave, with a frequency shift $\Delta\omega_{\mathrm{NL}}$ due to a trapped particle distribution.

The damping rate in (6.2) has a weaker scaling than that predicted by Zakharov & Karpman (1963). Their derivation results in a ω_B^{-3} scaling, while the best fit finds a weaker scaling of $\omega_B^{-1.48}$. Due to this, the ZK damping rate significantly underestimates the observed damping rate for large ω_B. This could be because ZK uses a perturbative approach that assumes strong trapping such that $\omega_B \gg \nu_{ee} v_{th}^2 / v_{tr}^2$, which may not hold for weaker wave amplitudes. Similar to the nonlinear frequency shift, it might be that ω_B^{-3} scaling would be more accurate for much larger wave amplitudes and at smaller wavenumbers.

Simulations show that the EPW persists in Phase II for $> \mathcal{O}(10)$ trapping oscillations. The lifetime of the quasi-steady state during Phase II can also be characterised and an empirical fit is provided in (6.3).

7. Phase III: return to Landau damping

Phase III begins when the distribution function has returned to a nearly Maxwellian state and the wave rapidly damps via Landau damping. As shown in figure 2(*a*), the damping rate increases rapidly to approximately the Landau damping rate (or slightly higher) and figure 2(*c*) shows that the oscillation frequency rapidly returns to a value near the initial ω_{EPW}.

7.1. *Distribution function thermalisation*

Figure 11(*a*) shows the total change in the spatially averaged distribution function over all three phases for Simulation C. During Phases I and II, there is an increase in density near the trapping velocity. During Phase III, this density increase has been erased and the additional phase space density has been redistributed to lower velocities as the distribution function returns to a Maxwellian.

Figure 11(*b*) shows the contribution to the susceptibility function from each term during Phase III. It shows that the Fokker–Planck term is responsible for returning

https://doi.org/10.1017/S0022377826101986 Published online by Cambridge University Press

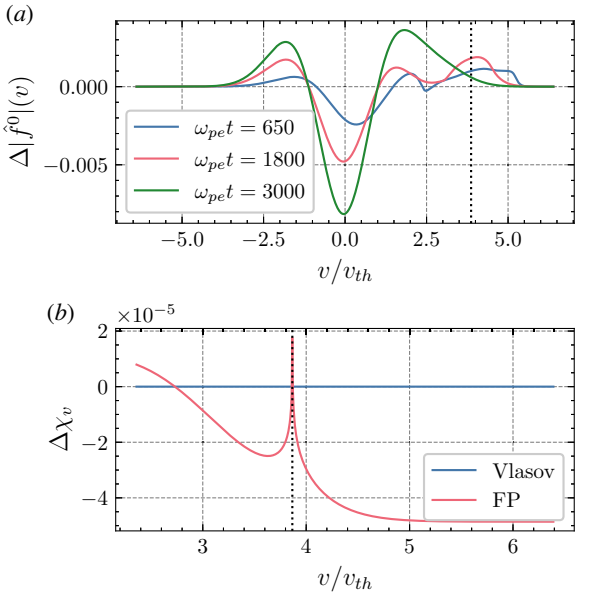


FIGURE 11. (*a*) $\Delta|\hat{f}^0(v)|$ accumulated through Phase I, Phase II and Phase III. (*b*) Contribution to $\Delta\chi(v)$ in phase III from each term.

the distribution function to a Maxwellian, while the effect of the Vlasov term is negligible.

7.2. *Wave properties and enhanced damping*

Finally, the Phase III dynamics are given by

$$f_{\mathrm{L}} = 1.73 \pm 0.18 \, \frac{\omega_B^{0.78\pm0.01} \, \nu_{ee}^{0.15\pm0.01}}{(k\lambda_D)^{2.25\pm0.06}}, \tag{7.1}$$

where f_L gives the damping rate as a multiple of the Landau damping rate in Phase III. It is seen that with more energy absorbed by the particles during Phase II (i.e. larger ω_B), the damping rate during Phase III is larger because the final Maxwellian is slightly warmer.

During Phase III, $\Delta\epsilon$ relaxes to a value smaller than the value at $t = 0$, suggesting a small frequency upshift. This upshift is likely due to the heating of the distribution function from absorbing the EPW energy. The return to a Maxwellian distribution is gradual during Phase III as the Fokker–Planck contribution asymptotically approaches the necessary value for the slightly warmer EPW.

8. Conclusion

This work presents a comprehensive kinetic study of large-amplitude electron plasma wave evolution in weakly collisional plasmas using 1600 Vlasov–Poisson–Fokker–Planck simulations spanning a broad parameter space in wavenumber, wave amplitude and collision frequency. The simulations reveal that the wave dynamics naturally partition into three distinct phases, each governed by different physical mechanisms and amenable to different perturbative descriptions.

https://doi.org/10.1017/S0022377826101986 Published online by Cambridge University Press

Phase I encompasses the well-understood collisionless dynamics of wave excitation, particle trapping and quasi-linear plateau formation. During this short-lived phase, the distribution function flattens at the phase velocity, wave damping is suppressed and a nonlinear frequency downshift emerges consistent with previous theoretical predictions, though with a weaker amplitude scaling ($\Delta\omega \propto \omega_B^{0.82}$) than the linear dependence predicted by asymptotic theory.

The central finding of this work concerns Phase II, during which a quasi-steady equilibrium develops between weak electron–electron collisions and strong wave–electron interactions. Counter-intuitively, collisions are found to enhance the nonlinear frequency shift rather than simply restore linear behaviour. This effect arises because the Fokker–Planck collision operator contributes positively to the susceptibility function, while the Vlasov terms only partially counteract this contribution. The frequency shift can approximately double during Phase II relative to its Phase I value. Empirical scaling relations for the initial frequency shift (5.1), frequency shift growth rate (6.1), effective damping rate (6.2) and phase lifetime (6.3) are provided, enabling the construction of reduced models for weakly collisional EPW dynamics.

A comparison of the damping rate in Phase II with Zakharov–Karpman theory reveals that while the linear scaling with collision frequency is confirmed, the theory underpredicts the damping rate by approximately an order of magnitude and predicts a stronger inverse dependence on bounce frequency (ω_B^{-3}) than is observed ($\omega_B^{-1.48}$).

Phase III marks the return to linear behaviour as collisions restore a near-Maxwellian distribution and the wave undergoes rapid Landau damping. The transition occurs after a time, τ_{II} given by (6.3), and the damping rate during this phase is characterised by (7.1)

Because this study is one-dimensional, it cannot capture transverse escape of trapped electrons from finite-width laser hot-spots ('sideloss'), often the dominant loss channel in inertial confinement fusion (ICF) geometries. Sideloss is commonly modelled as a Krook relaxation at rate $\nu_{\rm sl} \approx v_{\rm th}/L_\perp$ (Strozzi 2005). For an NIF-like single speckle ($L_\perp \approx 2.8\,\mu$m, $f/8$, 3ω) in plasma with $T_e = 3$ keV and $n_e/n_c = 0.1$, $\nu_{\rm sl}/\omega_{pe} \approx 5 \times 10^{-3}$, roughly an order of magnitude above the Phase II rate $\nu_{\rm eff}/\omega_{pe} \sim 6 \times 10^{-4}$ from (6.2) at representative parameters ($k\lambda_D = 0.3$, $\omega_B = 0.15$, $\nu_{ee} = 10^{-4}$), and also above the threshold $\sim 2 \times 10^{-3}\,\omega_{pe}$ at which Strozzi (2005) observed sharp disruption of trapping. At the single-speckle scale, sideloss is therefore expected to dominate, and the 1-D Phase II time scales reported here would overestimate the persistence of the nonlinear state. The two rates become comparable for $L_\perp \gtrsim 20\,\mu$m (a few speckle widths), and other geometric or kinetic loss channels may dominate in space, ionospheric and discharge plasmas. The two mechanisms act through different phase-space channels. Krook sideloss damps deviations from a Maxwellian indiscriminately, whereas Fokker–Planck collisions preferentially diffuse the sharp separatrix gradients. A quantitative assessment of their competition is left to future work.

The collisional modification of the EPW dispersion relation reported here parallels recent findings for ion-acoustic waves (IAWs). For linear IAWs in laser-heated, non-Maxwellian plasmas, Capdessus *et al.* (2025) showed that binary Coulomb collisions modify both the real frequency and the damping rate. The Langdon-effect contribution and the collision-induced anisotropy contribution act in opposing directions, yielding damping rates either above or below the collisionless Landau rate. The Phase II results here add a nonlinear counterpart: the Fokker–Planck contribution

https://doi.org/10.1017/S0022377826101986 Published online by Cambridge University Press

to the susceptibility enhances the nonlinear frequency shift and produces an effective damping rate well above ν_{ee}. Together, these results suggest that dispersion in weakly collisional plasmas cannot be captured by the collisionless dispersion relation alone, nor by treating collisions as a simple relaxation towards a Maxwellian.

Future work should extend this analysis to explore the role of ion dynamics and investigate the interaction of multiple EPW modes in the weakly collisional regime. Additionally, developing analytic theory that captures the enhanced frequency shift mechanism identified here would provide deeper physical insight into the quasi-steady collisional dynamics of Phase II.

Acknowledgements

A.J. thanks useful discussions with B. Afeyan to motivate this study.

Editor Antoine C. Bret thanks the referees for their advice in evaluating this article.

Funding

This material is based upon work supported by IFE COLoR under U.S. Department of Energy Grant No. DE-SC0024863, US DOE National Nuclear Security Administration (NNSA) Center of Excellence under Cooperative Agreement No. DE-NA0003869, and by the Department of Energy National Nuclear Security Administration under Award Number DE-NA0004144, the University of Rochester, and the New York State Energy Research and Development Authority. This research used resources of the National Energy Research Scientific Computing Center, a DOE Office of Science User Facility supported by the Office of Science of the U.S. Department of Energy under Contract No. DE-AC02-05CH11231 using NERSC award FES-ERCAP0026741.

Declaration of interests

The authors report no conflict of interest.

REFERENCES

BÉNISTI, D. 2017*a* Nonlocal adiabatic theory. I. The action distribution function. *Phys. Plasmas* **24**, 092120.

BÉNISTI, D. 2017*b* Nonlocal adiabatic theory. II. Nonlinear frequency shift on an electron plasma wave in a multidimensional inhomogeneous plasma. *Phys. Plasmas* **24**, 092121.

BÉNISTI, D., STROZZI, D.J., GREMILLET, L. & MORICE, O. 2009 Nonlinear Landau damping rate of a driven plasma wave. *Phys. Rev. Lett.* **103**, 155002.

BERGER, R.L., ARRIGHI, W., CHAPMAN, T., DIMITS, A., BANKS, J.W. & BRUNNER, S. 2023 The competing effects of wave amplitude and collisions on multi-ion species suppression of stimulated Brillouin scattering in inertial confinement fusion *Hohlraums*. *Phys. Plasmas* **30**, 042715.

BERGER, R.L., BRUNNER, S., CHAPMAN, T., DIVOL, L., STILL, C.H. & VALEO, E.J. 2013 Electron and ion kinetic effects on non-linearly driven electron plasma and ion acoustic waves. *Phys. Plasmas* **20**, 032107.

BERNSTEIN, I.B., GREENE, J.M. & KRUSKAL, M.D. 1957 Exact nonlinear plasma oscillations. *Phys. Rev.* **108**, 546–550.

CANOSA, J. 1973 Numerical solution of Landau's dispersion equation. *J. Comput. Phys.* **13**, 158–160.

CAPDESSUS, R., RUYER, C., DEBAYLE, A., LOISEAU, P. & MASSON-LABORDE, P.E. 2025 Influence of collisional effects on ion-acoustic wave properties in non-maxwellian laser-driven plasmas. *Phys. Rev. Lett.* **135**, 125101.

DAVIDSON, R. 2012 *Methods in Nonlinear Plasma Theory*. Elsevier.

DEWAR, R.L. 1972 Frequency shift due to trapped particles. *Phys. Fluids* **15**, 712–714.

https://doi.org/10.1017/S0022377826101986 Published online by Cambridge University Press

DODIN, I.Y. 2014 On variational methods In the physics of plasma waves. *Fusion Sci. Technol.* **65**, 54–78.

DODIN, I.Y. & FISCH, N.J. 2012*a* Adiabatic nonlinear waves with trapped particles. I. General formalism. *Phys. Plasmas* **19**, 012102.

DODIN, I.Y. & FISCH, N.J. 2012*b* Adiabatic nonlinear waves with trapped particles. II. Wave dispersion. *Phys. Plasmas* **19**, 012103.

DODIN, I.Y. & FISCH, N.J. 2012*c* Adiabatic nonlinear waves with trapped particles. III. Wave dynamics. *Phys. Plasmas* **19**, 012104.

DOUGHERTY, J.P. 1964 Model Fokker-Planck equation for a plasma and its solution. *Phys. Fluids* **7**, 1788.

JOGLEKAR, A. & LEVY, M. 2020 VlaPy: a Python package for Eulerian Vlasov-Poisson-Fokker-Planck simulations. *J. Open Source Softw.* **5**, 2182.

JOGLEKAR, A.S. & THOMAS, A.G.R. 2023 Machine learning of hidden variables in multiscale fluid simulation. *Mach. Learn.: Sci. Technol.* **4**, 035049.

LANDAU, L.D. 1946 On the vibrations of the electronic plasma. *Zh. Eksp. Teor. Fiz.* **10**, 25.

LENARD, A. & BERNSTEIN, I.B. 1958 Plasma oscillations with diffusion in velocity space. *Phys. Rev.* **112**, 1456–1459.

MANHEIMER, W.M. & FLYNN, R.W. 1971 Formation of stationary large amplitude waves in plasmas. *Phys. Fluids* **14**, 2393–2396.

MORALES, G.J. & O'NEIL, T.M. 1972 Nonlinear frequency shift of an electron plasma wave. *Phys. Rev. Lett.* **28**, 417–420.

O'NEIL, T. 1965 Collisionless damping of nonlinear plasma oscillations. *Phys. Fluids* **8**, 2255.

STROZZI, D.J. 2005 Vlasov simulations of kinetic enhancement of raman backscatter in laser fusion plasmas. PhD thesis, Massachusetts Institute of Technology.

THOMAS, A.G.R. 2016 Vlasov simulations of thermal plasma waves with relativistic phase velocity in a Lorentz boosted frame. *Phys. Rev. E* **94**, 053204.

THORNE, K.S. & BLANDFORD, R.D. 2017 *Modern Classical Physics: Optics, Fluids, Plasmas, Elasticity, Relativity, and Statistical Physics*. Publisher Princeton University Press.

VALENTINI, F. 2008 Damping of Bernstein–Greene–Kruskal modes in collisional plasmas. *Phys. Plasmas* **15**, 022102.

ZAKHAROV, V.E. & KARPMAN, V.I. 1963 On the nonlinear theory of the damping of plasma waves. *Sov. J. Exp. Theor. Phys.* **16**, 351–357.

https://doi.org/10.1017/S0022377826101986 Published online by Cambridge University Press